ARTICLES

Mediterranean Botany
ISSNe 2603-9109

EDICIONES COMPLUTENSE

https://doi.org/10.5209/mbot.81561

Evaluating canopy water content in grasslands using in situ hyperspectral data: A case from the Eastern Mediterranean, Turkey

Ahmet Karakoç[1] & Murat Karabulut[2]

Received: 18 April 2022 / Accepted: 22 June 2023 / Published online:20 May 2024

Abstract. The water content of vegetation is considered a key parameter for ecological analysis and agricultural and forestry applications. Remote sensing techniques provide substantial benefits over conventional field methods in determining vegetation water content at the leaf, canopy, and landscape scales. This study evaluated the potential of hyperspectral vegetation indices in predicting canopy water content in grasslands. Data was gathered from three different grasslands situated at approximately 500 m asl, 1200 m asl, and 1400 m asl elevations. Each study area provided 71 samples, and a total of 213 samples were analyzed. In this context, 59 ratio-based hyperspectral vegetation indices were tested. The correlation between hyperspectral vegetation indices and canopy water content was evaluated using linear, exponential, logarithmic, and power regression models. The results showed that the NW-3 (920,970) index significantly represents the canopy water content variable. It was determined that the exponential regression model created with this index could explain the variations in canopy water content up to 85%.

On the other hand, it has been detected that the high level of water content in the vegetation creates a significant saturation problem. Another finding of this study is that the predictive power reaches higher levels in low canopy water content characteristics. The results of this study show that in situ hyperspectral data has a very high potential in determining vegetation water content in grasslands.

Keywords: Canopy water content, grasslands, hyperspectral remote sensing, vegetation indices, canopy reflectance.

How to cite: Karakoç, A. & Karabulut, M. 2024. Evaluating canopy water content in grasslands using in situ hyperspectral data: A case from the Eastern Mediterranean, Turkey. Mediterr. Bot. 45(2), e81561. https://doi.org/10.5209/mbot.81561

Introduction

Grasslands, which span over one-third of the Earth's land surface, contribute diverse ecosystem services such as food production, carbon sequestration, climate change mitigation, biodiversity preservation, water resource conservation, forage availability, and the potential for tourism and recreation (Andrade *et al*., 2015; Bangira *et al*., 2023; Blair *et al*., 2014; Zhao, 2023). Throughout Europe, from low-lying areas to mountainous areas, nearly all regions have semi-natural dry grasslands and scrubland habitats on calcareous substrates, which include rangelands, meadows, pastures, and fodder crops, is closely linked to the practice of extensive grazing and land use (Varela & Robles-Cruz, 2016). Despite having lower species diversity at larger spatial scales, Temperate Europe encompasses specific habitats with remarkably rich species composition on smaller scales, such as the semi-natural grasslands that are particularly characterized by their high vascular plant diversity (Habel *et al*., 2013).

The current diversity of the Mediterranean Basin, including the richness of its grasslands on a small scale, can be attributed not only to its favorable climatic conditions throughout history, including the Pleistocene glaciations, but also to the impact of human activities and the presence of a diverse landscape with isolated mountains and islands (Apostolova *et al*., 2014; Olmeda *et al*., 2019). Despite their ecological, cultural, and agricultural significance, grasslands are globally endangered due to various human-induced factors and climate change (Grašič *et al*., 2023). Especially high-mountain plant communities face a threat to their survival due to various causes, all of which originate from human activities and can be categorized as part of the phenomenon referred to as global change (Gavilán *et al*., 2012). Even significant changes in temperature and precipitation are projected to occur, thereby leading to marked transformations in high mountain ecosystems across southern Europe due to the impact of climate change (Gutiérrez-Girón & Gavilán, 2013).

Examining the biophysical and biochemical parameters of the dominant vegetation of these grasslands provides crucial information about the ecosystem's functionality. These parameters play a key role in various issues, such as calculating grazing productivity (Dong *et al*., 2020),

[1] Department of Geography, Kadirli Faculty of Humanities and Social Sciences, Osmaniye Korkut Ata University, Osmaniye, Turkey. Email: ahmetkarakoc@osmaniye.edu.tr
[2] Department of Geography, Faculty of Humanities and Social Sciences, Kahramanmaraş Sütçü İmam University, Kahramanmaraş, Turkey.

monitoring grazing health and vigor (Xu *et al*., 2019), preparing conservation plans for habitat and biodiversity (Monteiro *et al*., 2018), and determining land use strategies (Guo *et al*., 2000). Therefore, investigating the spatio-temporal variations of these properties will yield crucial insights into understanding vegetation growth, evaluating vegetation physiological conditions, and supporting ecosystem conservation. (Lu *et al*., 2017).

Vegetation water content (VWC) provides essential information for agricultural decisions, including the amount and timing of irrigation (Xu *et al*., 2020) or drought monitoring (Gao *et al*., 2014; Kowalski *et al*., 2023), as water stress often restricts photosynthesis and plant primary productivity (Zhang, & Zhou, 2019). Moreover, it provides crucial knowledge into various fire behavior prediction models and fire danger indices (Yebra *et al*., 2018), as it affects ignition, combustion, fuel availability, fire severity and propagation, and smoke composition and production (Colombo *et al*., 2008; Jackson *et al*., 2004; Liu *et al*., 2016; Yebra *et al*., 2013).

VWC analyses are traditionally carried out using data collected from the fieldwork (Le Vine & Karam, 1996). Extensive field surveys and laboratory procedures are applied in these studies, which have a high local level of accuracy but are time consuming and costly (Sibanda *et al*., 2019). Besides, it is often necessary to use interpolation methods to fill the temporal and spatial gaps of the obtained local data (Mendiguren *et al*., 2015). On the other hand, remote sensing methods are a powerful alternative for acquiring data at a wide variety of spatial and temporal scales (Bellini *et al*., 2023; Yuan *et al*., 2023). The surface reflectance can be measured directly in the field using spectroradiometers (Karakoç & Karabulut, 2019) or estimated through satellite imagery (Lei *et al*., 2023).

Several methods have been developed based on remote sensing studies of vegetation water content (Lei *et al*., 2023), which include: 1) spectral vegetation index methods (Solgi *et al*., 2023; Wang *et al*., 2009), 2) radar vegetation index methods (Mandal *et al*., 2020), 3) the PROSPECT and PROSAIL model (Jacquemoud *et al*., 2009; Ravi *et al*., 2022), 4) Canopy Equivalent Water Thickness (Meiyan *et al*., 2022), 5) intelligent algorithms (Zahid *et al*., 2019), and 6) the grey-level co-occurrence matrix method (GLCM) (Iqbal *et al*., 2021).

Although conducting in situ measurements can be time-consuming and costly, they provide the most dependable information for a specific date and present researchers with an opportunity to gain a comprehensive understanding of the studied environment (Frank *et al*., 2022). In recent years, a significant effort has been made to determine the water content at the canopy level using in situ remotely sensed data (Feng *et al*., 2023; Frank *et al*., 2022; García-Haro *et al*., 2020). These research studies are based on two approaches: a physically based approach and a statistical one (Liang, 2004). The physically based approach is a deductive research method that assumes that hyperspectral sensors perceive the light influenced by various canopy characteristics, including canopy architecture, structure, and composition (He & Mui, 2010). The statistical approach, commonly referred to as the empirical approach, is an inductive research method that investigates the existence of consistent correlations between variables derived from field measurements and spectral data (Darvishzadeh, 2008; Fan *et al*., 2018; Kycko *et al*., 2019; Tong *et al*., 2023).

The statistical applications are based on monitoring the change of water absorption area in the near-infrared (NIR) (780–1400 nm) and shortwave infrared (SWIR) (1400–3000 nm) regions of the spectrum. Variations in VWC can be observed in the changes in the absorption points centered at 970, 1200, 1450, 1940 and 2500 nm (Liu *et al*., 2016). However, several factors control this variability, such as vegetation type, canopy structure and ecological conditions. Since the variations are centered on specific bands, researchers are increasingly interested in hyperspectral data tools due to their capacity to collect data in hundreds of bands. Hence, hyperspectral data are widely used in the investigation of the biophysical and biochemical properties of vegetation (Danson & Bowyer, 2004; Colombo *et al*., 2008; Karakoç & Karabulut, 2019). Here, airborne and satellite-born sensors provide data for landscape-level analysis, while portable/handheld spectroradiometers are preferable for leaf or canopy-level surveys.

The main objective of this study is to investigate the relationships between the spectral characteristics of grasslands and the CWC using a handheld spectroradiometer and data collected by field studies. Thus, the performance of hyperspectral vegetation indices in estimating CWC in grasslands will be evaluated with a statistical approach. In this context, the research questions are: (1) Which hyperspectral vegetation index correlates highest with CWC? (2) How do CWC characteristics of grasslands affect model predictions?

Materials and Methods

Study area

Mediterranean calcareous grasslands are characterized by a high diversity of plant species adapted to dry and hot climatic conditions. These grasslands are known for their unique composition, with a high proportion of grasses and herbaceous species. Additionally, they are important for supporting a variety of wildlife and contributing to soil conservation. However, calcareous grasslands in the Mediterranean region are considered one of the most endangered ecosystems due to human activities, including urbanization, agriculture, and overgrazing (Vié *et al*., 2009). Therefore, it is crucial to understand the ecological processes that support the functioning of these grasslands to conserve them.

Vegetation biophysical and biochemical structures in grasslands are impacted by the emergence of diverse ecological conditions across varying elevations (Montalvo *et al*., 1993). The assignment of study areas was based on elevation, and three distinct elevation steps were selected to represent different grassland conditions.

Figure 1. The study area.

Sampling areas at ~500 m asl, ~1200 m asl and ~1400 m asl altitudes are located within the provincial borders of Kahramanmaraş (Turkey) and on the easternmost edge of the Central Taurus Mountains.

The existence of ecological conditions that change depending on the elevation steps also affects the floristic composition (Atalay *et al*., 2014). The first study area, located at 500 m asl, is adjacent to the Kahramanmaraş meteorological station, where the annual average temperature is 16.7 °C, and the total yearly precipitation is 731.3 mm. Intensive grazing activities occur in this area, connected to the city and livestock-based settlements. The vegetation cover in the region appears sparse and exhibits lower biomass characteristics (718 g m^{-2}) compared to other study areas (Karakoç, 2019). According to Varol (2003) and Turkish Plants Data Service (TÜBİVES), the dominant species in the field at approximately 1200 m asl are *Hordeum bulbosum* L., *Agropyron sp*., *Convolvulus cantabrica* L., *Adonis microcarpa* DC., *Lactuca sp*., and *Fibigia eriocarpa* (DC.) Boiss. *Trifolium sp*., *Bromus arvensis* L., *Secale sp*., *Bellis perennis* L., and *Taraxacum crepidiforme* DC. can also be listed. The second (1200 m asl) and third (1400 m asl) study areas have similar ecological characteristics and are adjacent to the Andırın meteorological station, where the annual average temperature is 13°C, and the annual total precipitation is 1418 mm. These karstic fields, covered with dense species such as *Pinus brutia*, *Pinus nigra*, *Abies clicica*, *Cedrus libani*, and *Quercus cerris*, are characterized by grass formations with high biomass characteristics (1025 g m^{-2} for 1200 m asl; 1891 g m^{-2} for 1400 m asl) nestled within dolines (Karakoç, 2019). The dominant species in this formation are *Trifolium sp.*, *Bromus arvensis* L., *Secale sp*., *Bellis perennis* L., and *Taraxacum crepidiforme* DC. at ~1200 m asl, and *Hordeum bulbosum* L., *Secale sp*., *Aegilops speltoides* Tausch var. *speltoides*, and *Trifolium sp.* at ~1400 m asl. Additionally, *Agropyron sp*., *Cynosurus echinatus* L., and *Poa pratensis* L. can be listed (Varol, 2003). Despite the intensive engagement in recreational activities and transhumance practices within these fields, they are currently experiencing substantial grazing pressure (Doygun *et al*., 2021; Karabörk, 2019).

Field study

Two methods were used to collect the samples: the purposive sampling method and the line transect method. Because of the heterogeneous vegetation pattern at ~500 m asl, all samples were collected by purposive sampling method to avoid data that do not characterize the study area. At both ~1200 m asl and ~1400 m asl, 21 samples were obtained with the purposive sampling method, and 50 samples were obtained by the line transect method. Transect routes consist of two separate lines of 125 meters each. Data were collected from the roads at intervals of 5 meters. Ultimately, 213 samples, 71 from each study area, were obtained. All measurements were made within 50x50 cm quadrats.

The first step of the data collection process is recording spectral signatures from predetermined sampling locations. ASD FieldSpec® HandHeld spectroradiometer (Analytical Spectral Devices, Inc., Boulder, CO, USA) was used for this operation. The device can measure between 325–1075 nm at 1 nm intervals. Thus, spectral data were obtained in 751 spectral bands in each reading. Because the 25° field of view probe was used while reading spectra, measurements were made approximately 75 cm above the canopy (Karakoç & Karabulut, 2021). Weather conditions and the angle

of incidence of light are important for the precision of spectroradiometer measurements. Therefore, the measures were completed between 10:00 and 14:00, when the sun angle changes the least, on windless and less cloudy days. The process was calibrated, taking aprox. 10–15 measurements using a white calibration panel. By doing that, we avoided potential imbalances resulting from variations in lighting conditions.

After the measurements mentioned above were done, the vegetation in quadrats were cut from the ground level. Subsequently, the labeled samples were swiftly transported to the laboratory environment in ziplock bags, where precision balances were used to obtain their weight measurements. The first weighing operation is recorded as the fresh weight (Guo *et al*., 2005). Afterward, the samples were laid in a thin layer in the laboratory environment and left to dry by mixing every day for a week. After the drying process was completed, it was reweighed a second time, and recorded as dry weight. As a result of the above steps, formula 4 was used to calculate the CWC parameter.

Data Processing

VWC analyzes are performed by calculating three common parameters: Fuel moisture content (FMC), equivalent water thickness (EWT), and canopy water content (CWC) (Mendiguren *et al*., 2015).

$$FMC\ (\%) = \frac{W_{Fresh} - W_{Dry}}{W_{Dry}} * 100 \quad (1)$$

FMC is calculated by subtracting the dry weight (W_{Dry}) from the fresh weight (W_{Fresh}) of the vegetation, dividing the result by the dry weight, and then converting the result to percentage (%) by multiplying by 100. FMC is considered a critical variable for fire models, as it produces vital information about the starting point and/or spread of the fire (Liu *et al*., 2016). If the moisture weight (the result of W_{Fresh}- W_{Dry}) is divided by fresh weight, the obtained result is called "live FMC"; if divided by dry weight, it is called "dead FMC" (Quan *et al*., 2015). As the dead matter on the ground (litter) is affected by meteorological conditions, meteorological danger indices can be used to estimate FMC directly. On the other hand, Live FMC is more variable than dead FMC, as it is a product of the interaction between plant physiology and soil moisture conditions (Danson & Bowyer, 2004).

EWT is calculated with the following formula:

$$EWT\ (g/cm^2) = \frac{W_{Fresh} - W_{Dry}}{Area_{Leaf}} \quad (2)$$

It is obtained by subtracting the dry weight (W_{Dry}) from the fresh weight (W_{Fresh}) of the vegetation and dividing it by the leaf area $(Area_{Leaf})$. It can also be defined as a parameter that measures the water layer density per unit leaf area or the water mass per leaf area.

CWC (the preferred method for this study) is calculated using the following formulas:

$$CWC\ (g/cm^2) = EWT * LAI \quad (3)$$

or

$$CWC\ (g/cm^2) = \frac{W_{Fresh} - W_{Dry}}{Area_{Ground}} \quad (4)$$

CWC, which provides information on water content at the canopy level, can be described as a joint result of EWT and LAI. Based on this interaction, it can be obtained by multiplying EWT and LAI. Another calculation method is subtracting the dry vegetation weight from the fresh and dividing the result by the area measured $(Area_{Ground})$ (Mendiguren *et al*., 2015).

The analysis is based on two basic categories: according to the elevation step of the study areas (field-based) and the amount of CWC of the samples (quantity-based). The field-based category consists of three classes: ~500 m asl, ~1200 m asl and ~1400 m asl. This classification is based on the study areas located at different elevations; therefore, the vegetation will develop under the influence of unique ecological dynamics and have a unique character. However, the quantity-based categorization is based on the judgment that samples with similar amounts will have a similar relationship with light, regardless of which field they are obtained from. Within this scope, preliminary analyses were made (Karakoç & Karabulut, 2017) and it was observed that the threshold of 1000 g m^{-2} constitutes a significant break. So, regardless of which field it was collected from, the samples were divided into two classes representing low (0-1000 g m^{-2}) and high (1000+ g m^{-2}) CWC. The sensitivity of ratio-based vegetation indices to saturation effect is well-established (Jiang *et al*., 2006; Karakoç & Karabulut, 2019), and thus, another objective of this classification is to determine the threshold at which saturation effect becomes apparent.

Spectral curves provide valuable information for visual interpretation of the photosynthetic activities of vegetation. Therefore, spectral measurements were converted to reflection curves from the radiance data. Formula 5 was used for this transformation (Peddle *et al*., 2001).

$$R_{(\lambda)} = \frac{L_{(\lambda)}}{S_{(\lambda)}}\ x\ Cal_{(\lambda)}\ x\ 100 \quad (5)$$

Here $L_{(\lambda)}$; the radiant wavelength of the target, $S_{(\lambda)}$; the radiance value obtained from the calibration panel, $Cal_{(\lambda)}$; shows the calibration factor value. By multiplying the result by 100, the reflectance values are converted to percentages.

The relationships between CWC and spectral data were investigated using ratio-based vegetation indices. These indices are obtained by applying basic arithmetic operations to selected wavelengths each other. In this study, 59 indices were tested. Appendix 1 shows the list of all indices; Table 1 shows the formulas that best explain the variations in CWC.

Table 1. The fittest vegetation indices for the estimation of CWC.

Indices	Formula	Sources
Simple Ratio SR (550,800)	$\frac{R_{800}}{R_{550}}$	Buschman & Nagel, 1993
Simple Ratio SR (740,780)	$\frac{R_{780}}{R_{740}}$	Mistele & Schmidhalter, 2010
Normalized Water Index-3 NW-3 (920,970)	$\frac{R_{970} - R_{920}}{R_{970} + R_{920}}$	Prasad *et al*., 2007

Statistical Analysis

To evaluate characteristics of the data set, firstly, descriptive statistics were presented, then normality tests were applied. Skewness and kurtosis statistics and Kolmogorov-Smirnov and Shaphiro-Wilk tests were used to examine the normality of the datasets (Genceli, 2007). It is also known that Kolmogorov-Smirnov and Shaphiro-Wilk tests are more useful when the number of observations is less than 300 (Kim, 2013). If the results of the tests are significant, it indicates that the data set is significantly different from the normal distribution.

Spectral data were evaluated in two ways. The study employed two approaches for analyzing CWC: visual interpretation through spectral reflection curves and modeling via vegetation indices. The visual interpretation approach utilized spectral ranges commonly recognized as indicators of significant biophysical and biochemical properties. For example, focusing on the red region (~600–700 nm) in the reflection curve gives indirect information about which sample contains relatively more CWC can be obtained. On the other hand, preliminary information about the water content in the samples can be acquired by looking at the manner of the curves in the water absorption region at 970 nm. More details can be found in Lillesand *et al*. (2018) about wavelength behaviors under the control of vegetation characteristics.

Although the interpretation of spectral curves gives general information about vegetation and provides the opportunity to compare samples, it is insufficient for empirical inferences. Hence, regression analysis was performed using vegetation indices to model the variations occurring in the CWC. The first is the "model" dataset group, where the model will be built, and the second is the "test" dataset group were used to test the model function. The model group contains approximately 80% of the studied dataset, while the test group approximately 20%. To build regression models, *exponential, linear, logarithmic,* and *power* function models were tested, and the function with the highest coefficient of determination (R^2) was chosen as the fittest explanatory model (He *et al*., 2009; Jin *et al*., 2014). In this way, the unknown CWC parameter was modeled based on known index values.

As a standard statistical metric, root mean square error (RMSE) was used to control model performance (Chai & Draxler, 2014). Statistical significance was determined using an alpha of 0.05, and the data were analyzed with SPSS 14.0 for Windows (SPSS Inc., Chicago, IL).

$$RMSE = \sqrt{\frac{\sum_{i}^{n=1} (Y_i - Y_i')^2}{N}} \quad (6)$$

Y_i= the measured parameter,
Y_i'= predicted parameter,
N; the number of observations

Results

Descriptive Statistics and Normality Tests

In the field-based category, the mean CWC at ~1400 m asl is about twice that of ~1200 m asl and about two and a half times that of ~500 m asl (Table 2). The standard deviation is also at the highest value at ~1400 m asl. Both the standard deviation and the range are at the lowest values at ~1200 m asl, indicating that this class has a more homogeneous structure than the others. However, ~500 m asl has low CWC characteristics and extreme values. In quantity-based classes, the standard deviations are lower than the mean value.

For this reason, it can be considered that the data sets are close to the normal distribution. However, the number of observations between classes is different. According to Kolmogorov-Smirnov and Shapiro-Wilk tests, it was determined that no data class was homogeneous. In other words, the data used in the study are significantly different from the normal distribution (Table 2).

Spectral Curves

Natural or artificial objects can transmit, absorb, or reflect specific portions of electromagnetic radiation based on their physical and chemical properties. On the other hand, healthy plants with high water content stand out with their unique reflection properties when compared to other natural objects. As shown in Figure 2h, the reflection properties of healthy plants with high water content are distinguishable from other natural objects due to their low reflection in the blue and red regions (around 400–500 nm and 600–700 nm, respectively), high reflection in the green region (around 500–600 nm), and very high reflection in the near infrared region (around 740–1400 nm) (Karakoç, 2019).

Table 2. Descriptive statistics and tests of normality. Abbreviations are: (sig.), signification; sig. < 0.05: significant at 95% confidence interval; sig. < 0.01: significant at 99% confidence interval.

		Field-Based			Quantity-Based	
Descriptive statistics and parameters of normality (g m^{-2})		~500 m asl	~1200 m asl	~1400 m asl	0-1000 g $^{m-2}$	1000+ g m^{-2}
N		71	71	71	156	57
Mean		502	727	1356	481	1902
Median		276	619	998	424	1630
Std. Deviation		740	365	942	239	890
Range		3892	1699	4608	924	3900
Minimum		74	243	322	74	1031
Maximum		3966	1943	4930	998	4930
Quartiles	25	211	477	669	281	1213
	50	276	619	998	424	1630
	75	377	957	1883	632	2290
Kolmogorov-Smirnov (sig.)		0,00	0,00	0,00	0,00	0,00
Shapiro-Wilk (sig.)		0,00	0,00	0,00	0,00	0,00

The curve representing the ~500 m asl class shows that there is no significant peak between the blue and red region, although the highest mean reflectance of the visible region (~400–700 nm) occurs at the green wavelength (~500–600 nm) (Figure 2d). On the other hand, at ~1200 m asl and ~1400 m asl, the mean absorption in the blue (~400–700 nm) and red (~600–700 nm) regions increased noticeably, so the green region became a prominent peak. The individual curves of the samples display the difference between the red bottom regions at ~1200 m asl and ~1400 m asl is less than those at ~500 m asl (Figures 2a-2c). Moreover, as the elevation step of the study area increases, the absorption at the red bottom also increases. ~1400 m asl is the area where the curves converge the most in the visible region (Figure 2c). In the NIR region (~780–2500 nm), the highest mean reflection occurs at ~1400 m asl and the lowest at ~500 m asl (Figure 2c). At ~1200 and ~1400 m asl the absorption behavior centered at 970 nm (water absorption region) is much more apparent than at ~500 m asl (Figures 2a-2d).

The 1000+ g m^{-2} data class in the quantity-based categorization revealed a more homogeneous reflection characteristic in the visible region (Figure 2f). In the 0-1000 g m^{-2} class visible region reflectance are significantly higher and even exceed 20% in the red region (Figure 2e). Reflectance curves of both quantity-based data classes show that as the amount of CWC increases, the red absorption region becomes more pronounced and the variation between samples decreases. The variability of the curves in the NIR region is also quite evident. Although the lowest NIR reflection is around 20% in the 0-1000 g m^{-2} class, this rate is around 40% in the 1000+ g m^{-2} class and the maximum reflections have reached up to 90%. The 0-1000 g m^{-2} class curve shows higher reflectance values throughout the visible region, including the red-edge region (~680–750 nm). However, after about 700 nm, the situation reverses and the 1000+ g m^{-2} class shows higher reflection trend.

While the visual interpretation of the spectral curves provides useful information in terms of comparing data classes and the samples, it is necessary to quantitative analyzis on vegetation indices to reach empirical findings.

Vegetation Indices

Ratio-based vegetation indices were used to analyze the relationships between CWC and spectral data. At first, regression models were produced by using vegetation indices, and then CWC estimations were made based on the model functions. About 80% of the data set was used for building and 20% for testing the model. Fifty-nine vegetation indices were analyzed in this process. All tested indices and the coefficient of determination are given in Appendix 1.

According to the regression models, the NW-3 (920.970) index produced the strongest function for all samples in all categories (Table 3). The *exponential* function created with this index has an explanatory power of 74% for the variations in CWC (Figure 3a). However, as the amount of CWC increases, the scattering points become distant from the regression curve. This case can be considered as a clear indication of the saturation problem. The estimation model also shows that errors increase especially in samples over 1000 g m^{-2} (Figure 3b).

Analysis for the field-based category showed that NW-3 (920,970) was the most suitable vegetation index for CWC estimation at ~500 m asl. The power of the *exponential* model created with this index to explain the variations in the CWC is over 84% (Figure 4a). However, it was observed that the predictive power decreased considerably in samples above 1000 g m^{-2}. Up to this threshold, the clusters of scattering points around the curve can be considered as evidence that high CWC significantly affects the predictive power of the models. It was determined that the NW-3 (920,970) index was the fittest index in the models built for ~1200 m asl. The *exponential* model created with this index had an explanatory power of around 75% (Figure 4c).

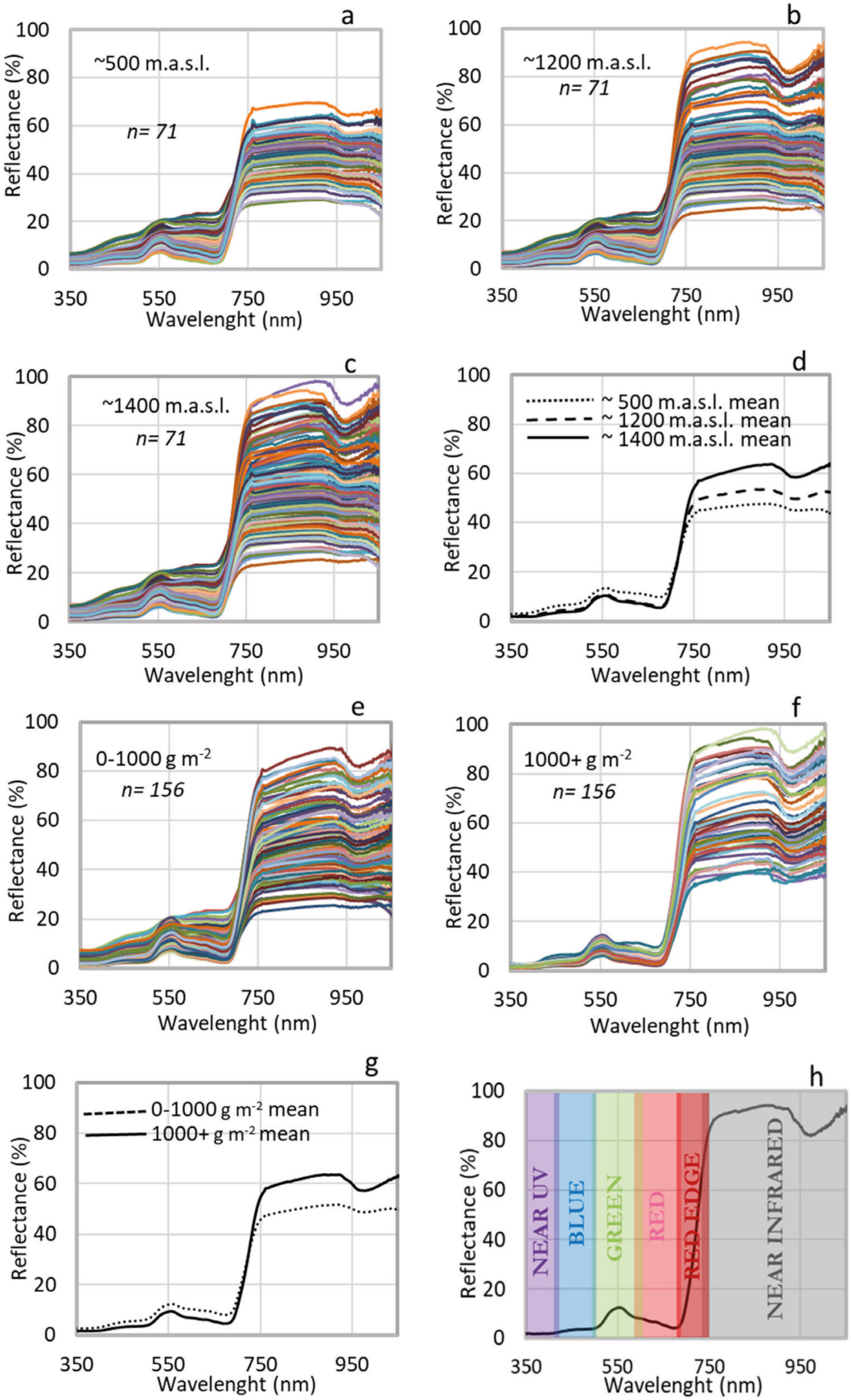

Figure 2. Spectral curves of field-based (a-d), quantity-based (e-g) classes and the typical reflection properties of healthy plants with high water content (h).

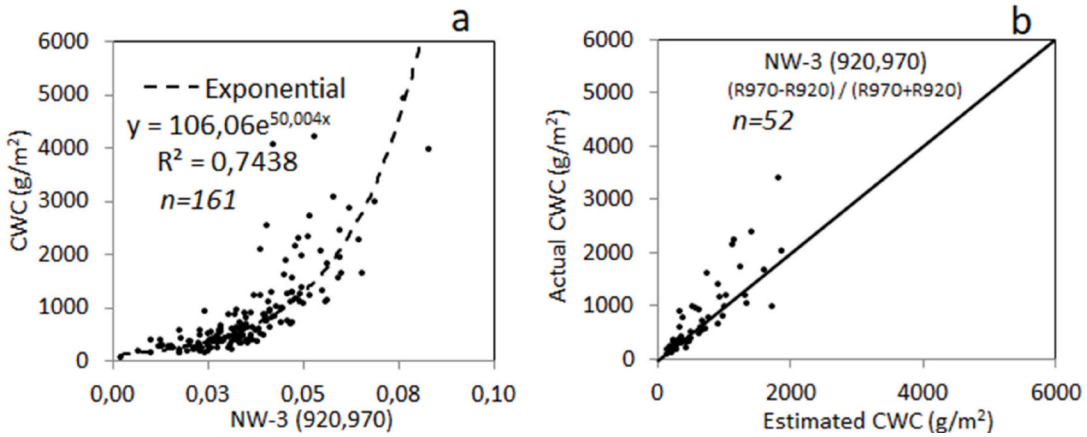

Figure 3. The fittest model function (a) and test of the model (b) for all samples in all categories.

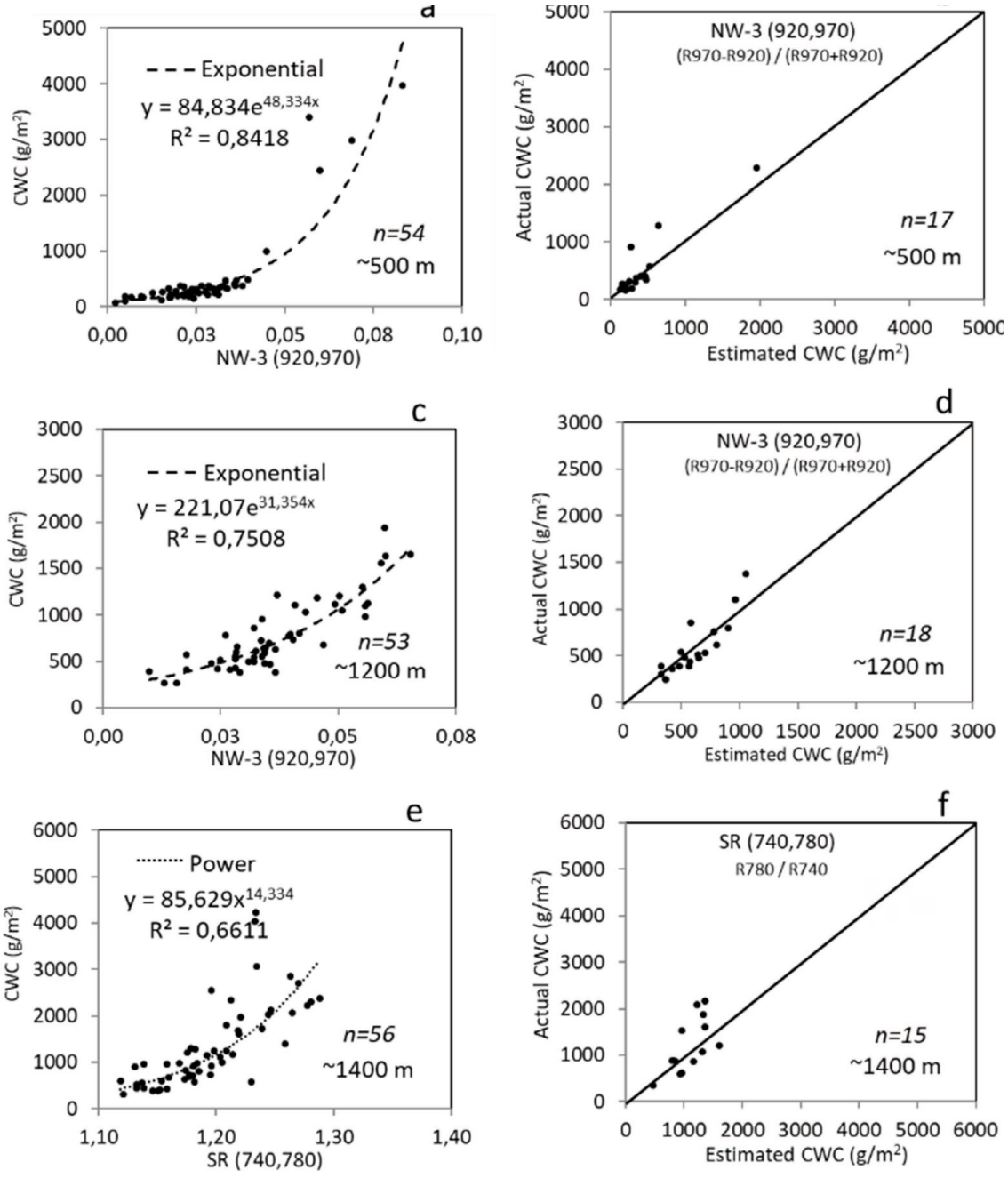

Figure 4. The fittest model function (a, c, e) and test of the model (b, d, f) for field-based classes.

Table 3. The most suitable models and corresponding RMSE values were determined for all categories and samples.

Category/Class		Indices	Model	R^2	Formula	RMSE (g m^{-2})
All samples		NW-3 (920,970)	*Exponential*	0,7438	$y = 106{,}06e^{50{,}004x}$	414
Field-based	~500 m asl	NW-3 (920,970)	*Exponential*	0,8418	$y = 84{,}834e^{48{,}334x}$	244
	~1200 m asl	NW-3 (920,970)	*Exponential*	0,7508	$y = 221{,}07e^{31{,}354x}$	151
	~1400 m asl	SR (740,780)	*Power*	0,6611	$y = 85{,}629x^{14{,}334}$	983
Quantity-based	0-1000 g m^{-2}	SR (550,800)	*Power*	0,6671	$y = 46{,}507x^{1{,}6005}$	152
	1000+ g m^{-2}	SR (740,780)	*Exponential*	0,4712	$y = 0{,}7039e^{6{,}4319x}$	202

For ~1400 m asl, unlike the other two fields, the *power* function has the highest explanation (Figure 4e). In this field, the model created with the SR (740.780) index reached an explanatory power of around 66%.

It has been determined that the most useful index for the CWC estimation of the 0-1000 gr/m^2 class is SR (550,800). The *power* function created with this index explains more than 66% of the variations in this data class, representing low CWC (Figure 5a). For the 1000+ g m^{-2} class, representing high CWC, SR (740,780) was the fittest index. The *exponential* function created with this index has an explanatory power of 47% for the variations occurring in CWC (Figure 5c). When the distribution of prediction points is examined, it is seen that the model has low accuracy but high precision (Figure 5d).

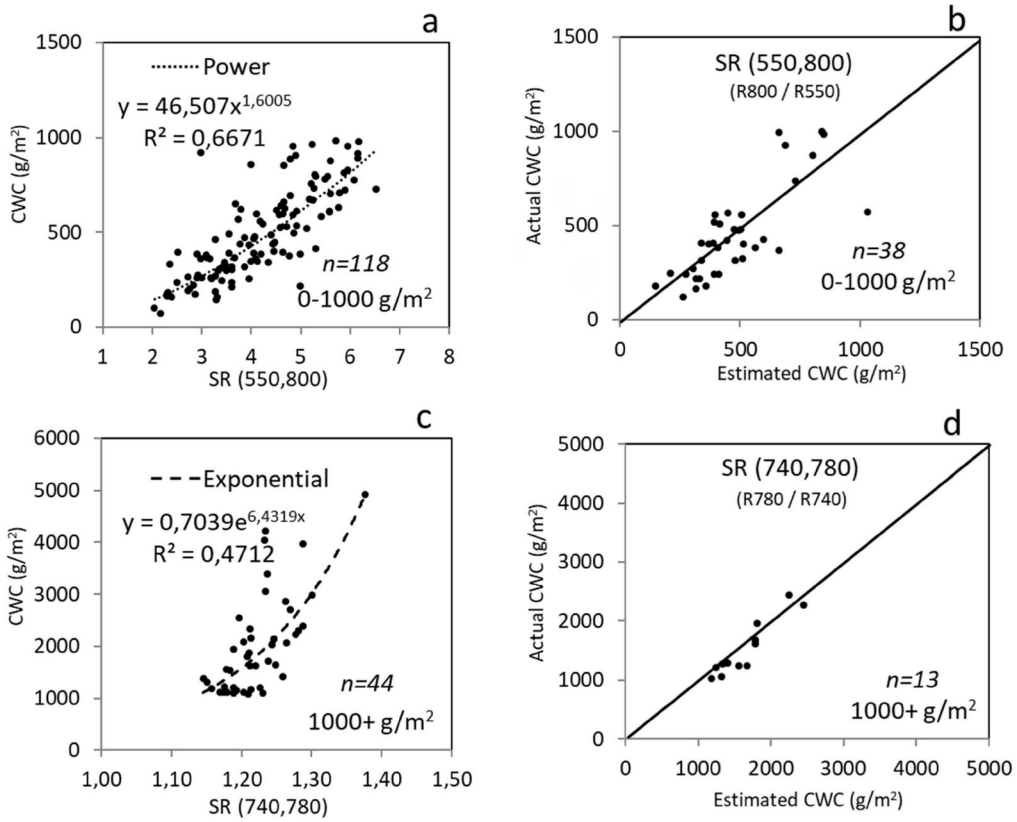

Figure 5. The fittest model function (a, c) and test of the model (b, d) for quantity-based classes.

Discussion

Diverse ecological conditions across different elevation gradient significantly influence the biophysical and biochemical structures of vegetation (Bora *et al*., 2020; Dechimo Jr & Buot Jr, 2023; Pescador *et al.,* 2015; Zou *et al*., 2023). In this context, there is an effort to test existing indices (Yang and Guo, 2014; Wu *et al*., 2008) or to produce new vegetation indices in studies conducted at the hyperspectral level (Chang-Hua *et al*., 2010; He *et al*., 2006; Jiang *et al*., 2022). The main reason for this is that vegetation indices are affected by many external factors and there is no linear relationship between the biophysical and biochemical properties of vegetation and vegetation indices (Xie *et al*., 2009). For example, in grasslands with low green vegetation density, NDVI is unstable due to soil color, canopy structure and atmospheric conditions. At the

same time, the Red Edge Position Index (REP) is less affected by these conditions (Cho *et al*., 2007). In addition, the problem of the decrease in the power of vegetation indices in areas with high green biomass, called the saturation phenomenon, leads researchers to search for various indices (Ren & Zhou, 2019; Zhao *et al*., 2014). The study areas were carefully chosen based on elevation gradient to observe these variations, resulting in three distinct elevation steps. These steps were selected to represent different grassland conditions and were located at approximately 500, 1200, and 1400 m asl in the easternmost region of the Central Taurus Mountains. This study aimed to examine the spectral VIs' potential for estimating CWC by using in situ hyperspectral data (Zhang & Zhou, 2019).

In this research, the findings showed that all samples, without categorizing, as well as the ~500 m asl and ~1200 m asl classes had a very high explanatory power. These successful models are provided with NW-3 (920,970) (Normalized Water Index-3) and exponential function. However, the explanatory power has decreased in the ~1400 m asl class, and the model function used has also differentiated. The mean moisture content of this field is two to two and a half times higher than other areas. Therefore, the saturation effect weakened the power of the prediction models (He, 2008; Zhao *et al*., 2014). Vescovo *et al*. (2012) documented that when phytomass values reached 100 g m^{-2}, spectral vegetation indices such as NDVI, MSR, and EVI exhibited saturation. EVI 2, RDVI, and WDRVI consistently displayed comparable performance characteristics, as reported in the same study. As Xu et al. (2020) reported, the correlation between green LAI and green NDVI highlights the saturation challenges encountered when estimating LAI using NDVI. This implies that while NDVI demonstrates the potential to estimate lower LAI values, it lacks sufficient capability to assess higher LAI values accurately. In this regard, there is still an intense effort in the literature to solve the saturation problem in estimating the biophysical properties of grasslands (Mutanga *et al*., 2023; Peng *et al*., 2020; Xu *et al*., 2020).

One outstanding result of this study is that the CWC variations occurring at ~500 m asl could be modeled quite satisfactorily (~85%). The characteristic features of this area are high heterogeneity and clustering of most of the data at low values below the average. When evaluated in this context, it is remarkable that the low CWC characteristics in the field has a positive effect for estimation models (Vescovo *et al*., 2012; Yebra *et al*., 2018; Zhang & Zhou, 2019). The CWC at ~1200 m asl is relatively more evenly distributed. The analyzes for this field also show that CWC with high homogeneity character can be successfully modeled using the exponential model created with NW-3 (920,970). The least successful prediction coefficient of this class is ~1400 m asl with ~66%. This field, characterized by a high range and high average, has been explained by the power function. The main reason for the low predictive power of the models is the saturation effect.

Another consequence of the study is that quantity-based classes have lower explanatory power than field-based classes. The unique character of each study field has caused it to expose a consistent spectral character within itself (He *et al*., 2020). In other words, even if the amount of CWC is similar, the spectral behavior of samples collected from different fields does not have a consistent form. In this study, ~1400 m asl, characterized by high CWC, could be modeled much more successfully than the class where direct high CWC samples (1000+ g m^{-2}) were brought together. As a result, considering each study field individually makes the plant-light relationship more predictable. In addition, recent studies indicate that the correlations between spectral water indices and plant water traits are extensively influenced by factors such as water stress, plant species, growing conditions, and phenological stages (Zhang & Zhou, 2019).

The findings from this research indicate that the NW-3 (920,970) and SR (740,780) indices show promise, and the use of in situ hyperspectral data is effective in identifying factors related to canopy water content (CWC) in grasslands. Additional studies should be conducted to explore the factors that drive substantial changes in these areas.

Conclusions

Quantifying green vegetation across space and time is a valuable tool for studying the health and function of grasslands, enabling us to enhance our understanding of how land use and climate change impact these ecosystems. In recent years, landscape-level analyses have begun with data obtained from multispectral satellite images, airborne sensors, and hyperspectral satellites. The fact that multispectral satellites can continuously collect data in large areas and are easily accessible to researchers makes studies on this subject even more important. However, the results of widespread studies are not yet at the desired level of success. The main reason is the inability to obtain spatial and temporal data with sufficient resolution in large areas for biophysical and biochemical parameters. This problem is tried to be overcome with airborne sensors placed on aircraft or various aircraft. However, this method is both costly and not easily accessible to researchers.

On the other hand, the hyperspectral data collected at the local scale constitute an important basis for the analyses made at the landscape scale. Therefore, there is still an intense effort to investigate local relationships between ground measurements and hyperspectral data. The local-scale findings to be obtained through these efforts will form the basis for future research on a regional and global scale.

Acknowledgments

This study was produced from Ahmet Karakoç Doctoral Thesis and supported by the Scientific Research Project Coordination Unit of Kahramanmaraş Sütçü İmam University, Project Number 2017-1-73D.

Authorship contribution

AK: Conceptualization; Data curation; Field study; Formal analysis; Research; Methodology; Visualization; First draft. MK: Conceptualization; Formal analysis; Management of the project; Methodology; Software; Supervision; Review and editing.

Conflict of interest

None

References

Andrade, B.O., Koch, C., Boldrini, I.I., Vélez-Martin, E., Hasenack, H., Hermann, J.M., Kollmann, J., Pillar, V.D. & Overbeck, G.E. 2015. Grassland degradation and restoration: a conceptual framework of stages and thresholds illustrated by southern Brazilian grasslands. Natureza & Conservação 13(2): 95–104. doi: 10.1016/j.ncon.2015.08.002

Apostolova, I., Dengler, J., Di Pietro, R., Gavilán, R.G. & Tsiripidis, I. 2014. Dry grasslands of Southern Europe: syntaxonomy, management and conservation. Hacquetia 13(1): 1–14. doi: 10.2478/hacq-2014-0015

Atalay, I., Efe, R. & Öztürk, M. 2014. Effects of topography and climate on the ecology of Taurus mountains in the Mediterranean region of Turkey. Procedia Soc. Behav. Sci. 120: 142–156. doi: 10.1016/j.sbspro.2014.02.091

Bangira, T., Mutanga, O., Sibanda, M., Dube, T & Mabhaudhi, T. 2023. Remote Sensing Grassland Productivity Attributes: A Systematic Review Remote Sens. 15(8): 2043. doi: 10.3390/rs15082043

Bellini, E., Moriondo, M., Dibari, C., Leolini, L., Staglianò, N., Stendardi, L., Filippa, G., Galvagno, M. & Argenti, G. 2023. Impacts of Climate Change on European Grassland Phenology: A 20-Year Analysis of MODIS Satellite Data. Remote Sens. 15(1): 218. doi: 10.3390/rs15010218

Blair, J., Nippert, J. & Briggs, J. 2014. Grassland Ecology. In: Monson, R.K. (Ed.). Ecology and the Environment; The Plant Sciences 8, Chapter 14. Pp. 389–423. Springer, New York.

Bora, Z., Xu, X., Angassa, A., Wang, Y. & Zhao, Y. 2020. Do herbaceous species functional groups have a uniform pattern along an elevation gradient? The case of a semi-arid savanna grasslands in Southern Ethiopia. International Int. J. Environ. Res. Public Health 17(8): 2817. doi: 10.3390/ijerph17082817

Buschman, C. & Nagel, E. 1993. In vivo spectroscopy and internal optics of leaves as a basis for remote sensing of vegetation. Int. J. Remote Sens. 14: 711–722. doi:10.1080/01431169308904370

Chai, T. & Draxler, R.R. 2014. Root mean square error (RMSE) or mean absolute error (MAE)? -Arguments against avoiding RMSE in the literature. Geosci. Model Dev. 7(3): 1247–1250. doi: 10.5194/gmd-7-1247-2014

Chang-Hua, J.U., Tian, Y., Yao, X., Cao, W., Zhu, Y. & Hannaway, D. 2010. Estimating Leaf Chlorophyll Content Using Red Edge Parameters. Pedosphere 20–25. doi: 1016/S10020160(10)60053-7

Cho, M.A., Skidmore, A.K., Corsi, F., van Wieren, S.E. & Sobhan, I. 2007. Estimation of green grass/herb biomass from airborne hyperspectral imagery using spectral indices and partial least squares regression. Int. J. Appl. Earth Obs. 9(4): 414–424. doi: 10.1016/j.jag.2007.02.001

Colombo, R., Meroni, M., Marchesi, A., Busetto, L., Rossini, M., Giardino, C. & Panigada, C. 2008. Estimation of leaf and canopy water content in poplar plantations by means of hyperspectral indices and inverse modeling. Remote Sens. Environ. 112(4): 1820–1834. doi: 10.1016/J.RSE.2007.09.005

Danson, F.M. & Bowyer, P. 2004. Estimating live fuel moisture content from remotely sensed reflectance. Remote Sens. Environ. 92(3): 309–321. doi: 10.3390/rs11131575

Darvishzadeh, R. 2008. Hyperspectral remote sensing of vegetation parameters using statistical and physical models. PhD Thesis. International Institute for Geo-information Science and Earth Observation (ITC), Enschede.

Dechimo Jr, A.A. & Buot Jr, I.E. 2023. Biophysical assessment of the plant biodiversity of Northern Negros Natural Park, Negros Island, Philippines. Biodiversitas 24(1). doi: 10.13057/biodiv/d240167

Dong, S., Shang, Z., Gao, J. & Boone, R.B. 2020. Enhancing sustainability of grassland ecosystems through ecological restoration and grazing management in an era of climate change on Qinghai-Tibetan Plateau. Agr. Ecosyst. Environ. 287: 106684. doi: 10.1016/j.agee.2019.106684

Doygun, H., Zülkadiroğlu, D. & Ekşi, I. 2021. Başkonuş Mesire Yeri'nden (Kahramanmaraş) Sağlanan Ekosistem Hizmetlerine Yönelik Algının İncelenmesi. Çukurova Tarım ve Gıda Bilimleri Dergisi 36(2): 219–230. doi: 10.36846/CJAFS.2021.50

Fan, L., Wigneron, J.P., Xiao, Q., Al-Yaari, A., Wen, J., Martin-StPaul, N., Dupuy, J.L, Pimont, F., Al Bitar, A., Fernandez-Moran, R. & Kerr, Y.H. 2018. Evaluation of microwave remote sensing for monitoring live fuel moisture content in the Mediterranean region. Remote Sens. Environ. 205: 210–223. doi: 10.1016/j.rse.2017.11.020

Feng, S., Qiu, J., Crow, W.T., Mo, X., Liu, S., Wang, S., Gao, L., Wang, X. & Chen, S. 2023. Improved estimation of vegetation water content and its impact on L-band soil moisture retrieval over cropland. J. Hydrol. 617: 129015. doi: 10.1016/j.jhydrol.2022.129015

Frank, T., Smith, A., Houston, B., Yang, X. & Guo, X. 2022. Estimating Biophysical Parameters of Native Grasslands Using Spectral Data Derived from Close Range Hyperspectral and Satellite Data. Can. J. Remote Sens. 48(5): 633–648. doi: 10.1080/07038992.2022.2088486

Gao, Z., Wang, Q., Cao, X. & Gao, W. 2014. The responses of vegetation water content (EWT) and assessment of drought monitoring along a coastal region using remote sensing. Gisci. Remote Sens. 51(1): 1–16. doi: 10.1080/15481603.2014.882564

García-Haro, F.J., Campos-Taberner, M., Moreno, Á., Tagesson, H.T., Camacho, F., Martínez, B., Sánchez, S., Piles, M., Camps-Valls, G., Yebra, M. & Gilabert, M.A. 2020. A global canopy water content product from AVHRR/Metop. ISPRS. J. Photogramm. 162: 77–93. doi: 10.1016/j.isprsjprs.2020.02.007

Gavilán, R.G., Díez-Monsalve, E., Izquierdo, J.L., Gutiérrez-Girón, A., Fernández-González, F. & Sánchez-Mata, D. 2012. An approach towards the knowledge of Iberian high-mountain calcareous grasslands. Lazaroa 33: 43–50. doi: 10.5209/rev_LAZA.2012.v33.40285

Genceli, M. 2007. Kolmogorov-Smirnov, Lilliefors and Shapiro-Wilk tests for normality. Sigma Journal of Engineering and Natural Sciences 25(4): 306–328.

Grašič, M., Šabić, A. & Lukač, B. 2023. A review of methodology for grassland restoration and management with practical examples. Acta Biologica Slovenica 66(1): 52–77. doi: 10.14720/abs.66.1.13230

Guo, X., Price, K.P. & Stiles, J.M. 2000. Modeling biophysical factors for grasslands in eastern Kansas using Landsat TM data. Transactions of the Kansas Academy of Science 103(3–4): 122–138. doi: 10.2307/3628261

Guo, X., Zhang, C., Wilmshurst, J.F. & Sissons, R. 2005. Monitoring grassland health with remote sensing approaches. In: Noble, B.F., Martz, D.J.F. & Aitken, A.E. (Eds.). Prairie Perspectives: Geographical Essays, vol. 8. Pp. 11–22. Department of Geography, University of Saskatchewan, Saskatoon.

Gutiérrez-Girón, A. & Gavilán, R.G. 2013. Plant functional strategies and environmental constraints in Mediterranean high mountain grasslands in central Spain. Plant Ecol. Divers. 6(3–4): 435–446. doi: 10.1080/17550874.2013.783641

Habel, J.C., Dengler, J., Janišová, M., Török, P., Wellstein, C. & Wiezik, M. 2013. European grassland ecosystems: threatened hotspots of biodiversity. Biodivers. Conserv. 22: 2131–2138. doi: 10.1007/s10531-013-0537-x

He, Y. & Mui, A. 2010. Scaling up semi-arid grassland biochemical content from the leaf to the canopy level: challenges and opportunities. Sensors-Basel. 10: 11072–11087. doi: 10.3390/ s101211072

He, Y. 2008. Modeling grassland productivity through remote sensing products. PhD Thesis. University of Saskatchewan, Saskatoon.

He, Y., Guo, X. & Wilmshurst, J.F. 2006. Studying mixed grassland ecosystems I: suitable hyperspectral vegetation indices. Can. J. Remote Sens. 32(2): 98–107. doi: 10.5589/m06-009

He, Y., Guo, X. & Wilmshurst, J.F. 2009. Reflectance measures of grassland biophysical structure. Int. J. Remote Sens. 30(10): 2509–2521. doi:10.1080/01431160802552751

He, Y., Yang, J. & Guo, X. 2020. Green vegetation cover dynamics in a heterogeneous grassland: spectral unmixing of Landsat time series from 1999 to 2014. Remote Sens. 12: 3826. doi: 10.3390/rs12223826

Iqbal, N., Mumtaz, R., Shafi, U. & Zaidi, S.M.H. 2021. Gray level co-occurrence matrix (GLCM) texture based crop classification using low altitude remote sensing platforms. PeerJ 7: e536. doi: 10.7717/peerj-cs.536

Jackson, T.J., Chen, D., Cosh, M., Li, F., Anderson, M., Walthall, C., Doriaswamy, P. & Hunt, E.R. 2004. Vegetation water content mapping using landsat data derived normalized difference water index for corn and soybean. Remote Sens. Environ. 92(4): 475–482. doi: 10.1016/j.rse.2003.10.021

Jacquemoud, S., Verhoef, W., Baret, F., Bacour, C., Zarco-Tejada, P.J., Asner, G.P., François, C. & Ustin, S.L. 2009. PROSPECT+ SAIL models: A review of use for vegetation characterization. Remote Sens. Environ. 113: 56–66. doi: 10.1016/j.rse.2008.01.026

Jiang, H., Yao, M., Guo, J., Zhang, Z., Wu, W. & Mao, Z. 2022. Vegetation monitoring of protected areas in rugged mountains using an improved Shadow-Eliminated Vegetation Index (SEVI). Remote Sens. 14(4): 882. doi: 10.3390/rs14040882

Jiang, Z., Huete, A.R., Li, J. & Chen, Y. 2006. An analysis of angle-based with ratio-based vegetation indices. IEEE T. Geosci. Remote 44(9): 2506–2513. doi: 10.1109/TGRS.2006.873205

Jin, Y., Yang, X., Qiu, J., Li, J., Gao, T., Wu, Q., Zhao, F., Ma, H., Yu, H. & Xu, B. 2014. Remote sensing-based biomass estimation and its spatio-temporal variations in temperate grassland, northern China. Remote Sens. 6: 1496–1513. doi: 10.3390/rs6021496

Karabörk, M. 2019. Başkonuş Dağının koruma kriterlerine göre değerlendirilmesi ve biyosfer rezervi açısından araştırılması. MA Thesis. Kahramanmaraş Sütçü İmam Universty, Institute of Social Sciences. Kahramanmaraş, Turkey.

Karabulut, M. 2018. An examination of spectral reflectance properties of some wetland plants in Göksu Delta, Turkey. J. Int. Environ. Appl. Sci. 13(4): 194–203.

Karakoç, A. & Karabulut, M. 2017. Otlaklarda kanopi nem içeriği tahmininde uygun vejetasyon indekslerinin belirlenmesi. Proceedings of the 3rd International Symposium on Social Science. Pp. 237–237. Kahramanmaraş.

Karakoç, A. & Karabulut, M. 2019. Ratio-based vegetation indices for biomass estimation depending on grassland characteristics. Turk. J. Bot. 43: 619–633. doi: 10.3906/bot-1902-50

Karakoç, A. & Karabulut, M. 2021. Estimating grassland chlorophyll content at canopy scales using hyperspectral vegetation indices. J Geog. 43: 77–91. doi: 10.26650/JGEOG2021-865289

Karakoç, A. 2019. Otlaklardaki Biyofiziksel Ve Biyokimyasal Özelliklerin Hiperspektral Uzaktan Algilama Verileri İle İncelenmesi. PhD Thesis. Kahramanmaraş Sütçü İmam Universty, Institute of Social Sciences, Kahramanmaraş.

Kim, H.Y. 2013. Statistical notes for clinical researchers: assessing normal distribution (2) using skewness and kurtosis. Restorative Dentistry and Endodontics 38(1): 52–54. doi: 10.5395/rde.2013.38.1.52

Kowalski, K., Okujeni, A. & Hostert, P. 2023. A generalized framework for drought monitoring across Central European grassland gradients with Sentinel-2 time series. Remote Sens. Environ. 286: 113449. doi: 10.1016/j.rse.2022.113449

Kycko, M., Zagajewski, B., Lavender, S. & Dabija, A. 2019. In situ hyperspectral remote sensing for monitoring of alpine trampled and recultivated species. Remote Sens. 11(11), 1296. doi: 10.3390/rs11111296

Le Vine, D.M. & Karam, M.A. 1996. Dependence of attenuation in a vegetation canopy on frequency and plant water content. IEEE T. Geosci. Remote 34(5): 1090–1096. doi: 10.1109/36.536525

Lei, J., Yang, W. & Yang, X. 2023. Estimation and Mapping of Aboveground Vegetation Water Storage in Jiuzhaigou Nature Reserve Using Sentinel Imagery. Pol. J. Environ. Stud. 32(1): 599–608. doi: 10.15244/pjoes/155052

Liang, S. 2004. Quantitative Remote Sensing of Land Surfaces, vol. 30. John Wiley & Sons, Hoboken.

Lillesand, T.M. & Kiefer, R.W. 1994. Remote Sensing and Image Interpretation John Wiley & Sons, Toronto.

Liu, L., Zhang, S. & Zhang, B. 2016. Evaluation of hyperspectral indices for retrieval of canopy equivalent water thickness and gravimetric water content. Int. J. Remote Sens. 37(14): 3384–3399. doi: 10.1080/01431161.2016.1199083

Lu, B., He, Y. & Liu, H.H. 2018. Mapping vegetation biophysical and biochemical properties using unmanned aerial vehicles-acquired imagery. Int. J. Remote Sens. 39(15–16): 5265–5287. doi: 10.1080/01431161.2017.1363441

Mandal, D., Kumar, V., Ratha, D., Dey, S., Bhattacharya, A., Lopez-Sanchez, J.M., McNairn, H. & Rao, Y.S. 2020. Dual polarimetric radar vegetation index for crop growth monitoring using sentinel-1 SAR data. Remote Sens. Environ. 247: 111954. doi: 10.1016/j.rse.2020.111954

Meiyan, S., Qizhou, D., ShuaiPeng, F., Xiaohong, Y., Jinyu, Z., Lei, M., Baoguo, L. & Yuntao, M. 2022. Improved estimation of canopy water status in maize using UAV-based digital and hyperspectral images. Comput. Electron. Agr. 197: 106982. doi: 10.1016/j.compag.2022.106982

Mendiguren, G., Pilar Martín, M., Nieto, H., Pacheco-Labrador, J. & Jurdao, S. 2015. Seasonal variation in grass water content estimated from proximal sensing and MODIS time series in a Mediterranean fluxnet site. Biogeosciences 12(18): 5523–5535. doi: 10.5194/bg-12-5523-2015

Mistele, B. & Schmidhalter, U. 2010. Tractor-based quadrilateral spectral reflectance measurements to detect biomass and total nitrogen in winter wheat. Agron. J. 102(2): 499–506. doi: 10.2134/agronj2009.0282

Montalvo, J., Casado, M.A., Levassor, C. & Pineda, F.D. 1993. Species diversity patterns in Mediterranean grasslands. J. Veg. Sci. 4(2): 213–222. doi: 10.2307/3236107

Monteiro, L., Machado, N., Martins, E., Pougy, N., Verdi, M., Martinelli, G. & Loyola, R. 2018. Conservation priorities for the threatened flora of mountaintop grasslands in Brazil. Flora 238: 234–243. doi: 10.1016/j.flora.2017.03.007

Mutanga, O., Masenyama, A. & Sibanda, M. 2023. Spectral saturation in the remote sensing of high-density vegetation traits: A systematic review of progress, challenges, and prospects. ISPRS J. Photogramm. Remote Sens. 198: 297–309. doi: 10.1016/j.isprsjprs.2023.03.010

Olmeda, C., Šefferová, V., Underwood, E., Millan, L., Gil, T. & Naumann, S. (compilers). 2019. EU Action plan to maintain and restore to favourable conservation status the habitat type 6210 Semi-natural dry grasslands and scrubland facies on calcareous substrates (Festuco-Brometalia) (*important orchid sites). European Commission Technical Report, Brussels.

Peddle, D.R., White, H.P., Soffer, R.J., Miller, J.R. & Ledrew, E.F. 2001. Reflectance processing of remote sensing spectroradiometer data. Comput. Geosci. 27: 203–213. doi: 10.1016/S0098-3004(00)00096-0

Peng, Y., Chen, H.Y. & Yang, Y. 2020. Global pattern and drivers of nitrogen saturation threshold of grassland productivity. Funct. Ecol. 34(9): 1979–1990. doi: 10.1111/1365-2435.13622

Pescador, D.S., de Bello, F., Valladares, F. & Escudero, A. 2015. Plant trait variation along an altitudinal gradient in Mediterranean high mountain grasslands: controlling the species turnover effect. PLoS One 10(3): e0118876. doi: 10.1371/journal.pone.0118876

Prasad, B., Carver, B.F., Stone, M.L., Babar, M.A., Raun, W.R. & Klatt, A.R. 2007. Potential use of spectral reflectance indices as a selection tool for grain yield in winter wheat under Great Plains conditions. Crop Sci. 47(4): 1426–1440. doi: 10.2135/cropsci2006.07.0492

Tong, X., Duan, L., Liu, T., Yang, Z., Wang, Y. & Singh, V.P. 2023. Estimation of grassland aboveground biomass combining optimal derivative and raw reflectance vegetation indices at peak productive growth stage. Geocarto Int. 38(1): 2186497. doi: 10.1080/10106049.2023.2186497

Quan, X., He, B., Li, X. & Tang, Z. 2015. Estimation of grassland live fuel moisture content from ratio of canopy water content and foliage dry biomass. IEEE Geosci. Remote. Sens. Lett. 12(9): 1903–1907. doi: 10.1109/LGRS.2015.2437391

Ravi, J., Nigam, R., Bhattacharya, B.K., Desai, D. & Patel, P. 2022. Retrieval of crop biophysical-biochemical variables from airborne AVIRIS-NG data using hybrid inversion of PROSAIL-D. Adv. Space Res. doi: 10.1016/j.asr.2022.11.047

Ren, H. & Zhou, G. 2019. Estimating green biomass ratio with remote sensing in arid grasslands. Ecol. Indic. 98: 568–574. doi: 10.1016/j.ecolind.2018.11.043

Sibanda, M., Mutanga, O., Dube, T., Mothapo, M.C. & Mafongoya, P.L. 2019. Remote sensing equivalent water thickness of grass treated with different fertiliser regimes using resample HyspIRI and EnMAP data. Phys. Chem. Earth. Pt. A/B/C 112: 246–254. doi: 10.1016/j.pce.2018.12.003

Solgi, S., Ahmadi, S.H. & Seidel, S.J. 2023. Remote sensing of canopy water status of the irrigated winter wheat fields and the paired anomaly analyses on the spectral vegetation indices and grain yields. Agr. Water Manage. 280: 108226. doi: 10.1016/j.agwat.2023.108226

Varela, E. & Robles-Cruz, A.B. 2016. Ecosystem services and socio-economic benefits of Mediterranean grasslands. In: Kyriazopoulos, A.P. López-Francos, A., Porqueddu, C. & Sklavou P. (Eds.). Options Mediterranéennes: Serie A. Mediterranean Seminars 114: 13–27.

Varol, Ö. 2003. Flora of Başkonuş Mountain (Kahramanmaraş). Turk. J. Bot. 27(2): 117–139.

Vescovo, L., Wohlfahrt, G., Balzarolo, M., Pilloni, S., Sottocornola, M., Rodeghiero, M. & Gianelle, D. 2012. New spectral vegetation indices based on the near-infrared shoulder wavelengths for remote detection of grassland phytomass. Int. J. Remote Sens. 33(7): 2178–2195. doi: 10.1080/01431161.2011.607195

Vié, J.C., Hilton-Taylor, C. & Stuart, S.N. (Eds.). 2009. Wildlife in a changing world: an analysis of the 2008 IUCN Red List of threatened species. IUCN.

Wang, J., Xu, R. & Yang, S. 2009. Estimation of plant water content by spectral absorption features centered at 1,450 nm and 1,940 nm regions. Environ. Monit. Assess. 157: 459–469. doi: 10.1007/s10661-008-0548-3

Wu, C. Y., Niu, Z., Tang, Q. & Huang, W. 2008. Estimating chlorophyll content from hyperspectral vegetation indices: modeling and validation. Agr. Forest Meteorol. 148(8–9): 1230–1241. doi: 10.1016/j.agrformet.2008.03.005

Xie, Y., Sha, Z., Yu, M., Bai, Y. & Zhang, L. 2009. A comparison of two models with Landsat data for estimating above ground grassland biomass in Inner Mongolia, China. Ecol. Model. 220(15): 1810–1818. doi: 10.1016/j.ecolmodel.2009.04.025

Xu, D., An, D. & Guo, X. 2020. The impact of non-photosynthetic vegetation on LAI estimation by NDVI in mixed grassland. Remote Sens. 12(12): 1979. doi: 10.3390/rs12121979

Xu, C., Qu, J.J., Hao, X., Cosh, M.H., Zhu, Z. & Gutenberg, L. 2020. Monitoring crop water content for corn and soybean fields through data fusion of MODIS and Landsat measurements in Iowa. Agr. Water Manage. 227: 105844. doi: 10.1016/j.agwat.2019.105844

Xu, S., Rowntree, J., Borrelli, P., Hodbod, J. & Raven, M.R. 2019. Ecological health index: A short term monitoring method for land managers to assess grazing lands ecological health. Environments 6(6): 67. doi: 10.3390/environments6060067

Yang, X. & Guo, X. 2014. Quantifying responses of spectral vegetation indices to dead materials in mixed grasslands. Remote Sens-Basel 6(5): 4289–4304. doi: 10.3390/rs6054289

Yebra, M., Dennison, P.E., Chuvieco, E., Riaño, D., Zylstra, P., Hunt Jr, E.R., Danson, M.F., Qi, Y. & Jurdao, S. 2013. A global review of remote sensing of live fuel moisture content for fire danger assessment: Moving towards operational products. Remote Sens. Environ. 136: 455–468. doi: 10.1016/j.rse.2013.05.029

Yebra, M., Quan, X., Riaño, D., Larraondo, P.R., van Dijk, A.I. & Cary, G. J. 2018. A fuel moisture content and flammability monitoring methodology for continental Australia based on optical remote sensing. Remote Sens. Environ. 212: 260–272. doi: 10.1016/j.rse.2018.04.053

Yuan, Z., Tong, S., Bao, G., Chen, J., Yin, S., Li, F., Chula, S. & Bao, Y. 2023. Spatiotemporal variation of autumn phenology responses to preseason drought and temperature in alpine and temperate grasslands in China. Sci. Total Environ. 859: 160373. doi: 10.1016/j.scitotenv.2022.160373

Zahid, A., Abbas, H.T., Ren, A., Zoha, A., Heidari, H., Shah, S.A., Imran, M.A., Alomainy, A. & Abbasi, Q.H. 2019. Machine learning driven non-invasive approach of water content estimation in living plant leaves using terahertz waves. Plant Methods 15(1): 1–13. doi: 10.1186/s13007-019 0522-9

Zhang, F. & Zhou, G. 2019. Estimation of vegetation water content using hyperspectral vegetation indices: A comparison of crop water indicators in response to water stress treatments for summer maize. BMC Ecol. 19: 1–12. doi: 10.1186/s12898-019-0233-0

Zhao, F., Xu, B., Yang, X., Jin, Y., Li, J., Xia, L., Shi, C. & Ma, H. 2014. Remote sensing estimates of grassland aboveground biomass based on Modis net primary productivity (NPP): a case study in the Xilingol grassland of Northern China. Remote Sens-Basel 6(6): 5368–5386. doi: 10.3390/rs6065368

Zhao, G. 2023. Trends in grassland science: Based on the shift analysis of research themes since the early 1900s. Fundamental Research 3(2): 201–208. doi: 10.1016/j.fmre.2022.05.008

Zou, L., Tian, F., Liang, T., Eklundh, L., Tong, X., Tagesson, T., Dou, Y., He, T., Liang, S. & Fensholt, R. (2023). Assessing the upper elevational limits of vegetation growth in global high mountains. Remote Sens. Environ. 286: 113423. doi: 10.1016/j.rse.2022.113423

Appendix 1. R^2 values for all tested indices (Karakoç, 2019).

INDICES	~500 m asl				~1200 m asl				~1400 m asl				0-1000 g m^{-2}				1000+ g m^{-2}			
	Exp.	Lin.	Log.	Pow.	Exp.	Lin.	Log.	Pow.	Exp.	Lin.	Log.	Pow.	Exp.	Lin.	Log.	Pow.	Exp.	Lin.	Log.	Pow.
SR (675,800)	0.630	0.552	0.356	0.520	0.502	0.455	0.459	0.538	0.103	0.062	0.083	0.134	0.489	0.506	0.518	0.568	0.000	0.003	0.007	0.000
SR (470,800)	0.706	0.609	0.416	0.598	0.627	0.586	0.531	0.626	0.119	0.051	0.055	0.129	0.592	0.594	0.586	0.643	0.001	0.000	0.001	0.000
SR (670,801)	0.637	0.567	0.356	0.527	0.505	0.457	0.462	0.541	0.112	0.071	0.091	0.143	0.492	0.509	0.520	0.570	0.000	0.004	0.009	0.001
SR (550,801)	0.732	0.663	0.499	0.647	0.733	0.679	0.628	0.706	0.390	0.245	0.249	0.399	0.648	0.635	0.613	0.667	0.043	0.073	0.057	0.033
SR (560,810)	0.729	0.666	0.496	0.642	0.731	0.676	0.625	0.705	0.383	0.242	0.246	0.392	0.647	0.634	0.611	0.666	0.040	0.071	0.055	0.031
SR (700,750)	0.641	0.549	0.394	0.548	0.628	0.578	0.545	0.621	0.284	0.188	0.199	0.303	0.525	0.514	0.503	0.552	0.012	0.027	0.029	0.014
SR (550,750)	0.721	0.634	0.480	0.637	0.722	0.664	0.613	0.694	0.354	0.213	0.218	0.362	0.650	0.635	0.611	0.666	0.012	0.031	0.024	0.009
SR (710,750)	0.639	0.538	0.428	0.571	0.681	0.633	0.599	0.669	0.428	0.302	0.304	0.434	0.521	0.498	0.492	0.539	0.085	0.111	0.108	0.085
SR (705,750)	0.641	0.543	0.411	0.561	0.661	0.611	0.576	0.649	0.357	0.243	0.249	0.369	0.528	0.510	0.501	0.549	0.036	0.057	0.057	0.037
SR (675,700)	0.378	0.207	0.246	0.412	0.373	0.297	0.296	0.367	0.000	0.000	0.001	0.000	0.540	0.426	0.477	0.524	0.021	0.005	0.008	0.028
SR (415,685)	0.192	0.183	0.153	0.168	0.011	0.013	0.011	0.009	0.148	0.174	0.163	0.146	0.010	0.012	0.013	0.011	0.044	0.071	0.065	0.037
SR (415,695)	0.000	0.016	0.013	0.000	0.234	0.163	0.168	0.237	0.270	0.329	0.286	0.245	0.345	0.326	0.282	0.296	0.119	0.145	0.135	0.108
G (554,677)	0.378	0.234	0.200	0.351	0.258	0.211	0.213	0.263	0.005	0.002	0.003	0.006	0.368	0.357	0.361	0.400	0.013	0.003	0.001	0.007
SR (550,800)	0.732	0.663	0.499	0.647	0.733	0.679	0.627	0.706	0.390	0.245	0.249	0.399	0.648	0.634	0.613	0.667	0.043	0.073	0.057	0.033
SR (670,700)	0.455	0.304	0.268	0.432	0.354	0.290	0.303	0.374	0.001	0.000	0.000	0.001	0.492	0.476	0.483	0.529	0.028	0.008	0.005	0.000
SR (720,740)	0.609	0.492	0.436	0.574	0.702	0.652	0.632	0.694	0.535	0.394	0.389	0.533	0.506	0.473	0.471	0.516	0.179	0.199	0.197	0.179
SR (650, 675,700)	0.620	0.566	0.439	0.545	0.000	0.004	0.004	0.000	0.270	0.533	0.535	0.300	0.145	0.118	0.115	0.151	0.023	0.038	0.058	0.039
SR (550,672,708)	0.019	0.006	0.004	0.024	0.291	0.254	0.286	0.293	0.105	0.058	0.066	0.108	0.174	0.182	0.200	0.194	0.024	0.022	0.039	0.042
SR (550,708,860)	0.778	0.766	0.516	0.672	0.181	0.128	0.143	0.196	0.320	0.193	0.228	0.368	0.456	0.441	0.446	0.514	0.038	0.067	0.077	0.048
SR (765,787)	0.012	0.059	0.059	0.012	0.000	0.004	0.004	0.000	0.120	0.097	0.097	0.120	0.141	0.137	0.138	0.142	0.083	0.066	0.066	0.083
SR (415,710)	0.385	0.164	0.183	0.401	0.454	0.344	0.404	0.513	0.219	0.316	0.290	0.205	0.615	0.536	0.534	0.576	0.218	0.220	0.215	0.214
SR (680,900)	0.627	0.545	0.352	0.515	0.500	0.449	0.456	0.536	0.094	0.055	0.075	0.125	0.489	0.514	0.525	0.576	0.001	0.002	0.006	0.000
SR (740,780)	0.666	0.636	0.611	0.653	0.709	0.703	0.702	0.713	0.659	0.552	0.551	0.661	0.500	0.463	0.465	0.506	0.471	0.471	0.466	0.471
VIopt1 (730,760)	0.629	0.551	0.504	0.601	0.704	0.676	0.666	0.704	0.639	0.528	0.522	0.639	0.459	0.422	0.425	0.469	0.414	0.425	0.417	0.413
DI1 (550,800)	0.275	0.194	0.161	0.240	0.507	0.561	0.522	0.522	0.006	0.006	0.010	0.008	0.330	0.327	0.335	0.351	0.002	0.004	0.000	0.000
PSSRa (680,800)	0.622	0.537	0.348	0.513	0.504	0.456	0.460	0.539	0.101	0.060	0.080	0.133	0.490	0.506	0.515	0.566	0.001	0.002	0.005	0.000
PSSRb (635,800)	0.675	0.628	0.416	0.567	0.587	0.538	0.522	0.603	0.228	0.160	0.175	0.255	0.543	0.549	0.542	0.594	0.011	0.028	0.032	0.014
CIG (550,800)	0.693	0.603	0.372	0.557	0.633	0.574	0.528	0.624	0.144	0.069	0.077	0.160	0.590	0.592	0.573	0.641	0.001	0.000	0.001	0.000
NDVI (680,800)	0.398	0.221	0.160	0.333	0.507	0.412	0.373	0.469	0.154	0.093	0.096	0.158	0.563	0.468	0.421	0.542	0.001	0.009	0.009	0.001
NDVI (635,800)	0.457	0.280	0.203	0.382	0.573	0.474	0.434	0.536	0.268	0.180	0.180	0.270	0.592	0.504	0.459	0.574	0.017	0.034	0.035	0.017
NDVI (470,800)	0.477	0.273	0.229	0.434	0.560	0.448	0.415	0.527	0.134	0.058	0.058	0.135	0.637	0.533	0.505	0.625	0.000	0.002	0.002	0.000
NDVI (430,680)	0.188	0.131	0.217	0.258	0.105	0.095	0.084	0.099	0.104	0.108	0.112	0.103	0.019	0.016	0.020	0.023	0.006	0.021	0.021	0.011
NDVI (550,801)	0.578	0.401	0.315	0.508	0.674	0.582	0.537	0.635	0.402	0.250	0.249	0.403	0.666	0.588	0.553	0.657	0.027	0.046	0.043	0.025
NDVI (670,801)	0.407	0.229	0.166	0.340	0.510	0.413	0.375	0.472	0.165	0.103	0.105	0.168	0.568	0.472	0.426	0.547	0.002	0.013	0.013	0.003
NDVI (680,710,750)	0.611	0.584	0.437	0.545	0.714	0.683	0.637	0.700	0.547	0.402	0.389	0.540	0.343	0.358	0.363	0.359	0.191	0.202	0.194	0.190
NDVI (705,750)	0.518	0.356	0.236	0.411	0.636	0.553	0.494	0.591	0.373	0.250	0.249	0.373	0.552	0.492	0.451	0.545	0.038	0.056	0.056	0.038
NDVI (445,705,750)	0.580	0.493	0.367	0.501	0.646	0.604	0.570	0.634	0.404	0.293	0.294	0.411	0.442	0.402	0.404	0.448	0.058	0.082	0.082	0.059
NDVI (531,570)	0.370	0.341	*	*	0.385	0.340	*	*	0.134	0.143	*	*	0.182	0.167	*	*	0.014	0.034	*	*
NDVI (531,550)	0.227	0.069	0.068	0.227	0.283	0.225	0.215	0.273	0.001	0.017	0.019	0.002	0.459	0.405	0.386	0.458	0.084	0.096	0.090	0.076
NDVI (440,573)	0.267	0.101	0.104	0.280	0.194	0.141	0.124	0.174	0.211	0.245	0.233	0.200	0.440	0.396	0.397	0.455	0.047	0.056	0.046	0.038
NDVI (533,565)	0.280	0.311	0.434	0.365	0.240	0.230	0.207	0.219	0.169	0.138	0.169	0.138	0.057	0.054	0.062	0.063	0.015	0.034	0.041	0.021
NDVI (483,503)	0.206	0.118	0.101	0.192	0.028	0.011	0.002	0.007	0.229	0.214	0.170	0.185	0.282	0.254	0.214	0.245	0.000	0.001	0.000	0.001
NDVI (708,760)	0.530	0.374	0.248	0.419	0.653	0.573	0.516	0.611	0.423	0.269	0.290	0.419	0.542	0.484	0.446	0.537	0.087	0.109	0.106	0.086
NDVI2 (600,800)	0.487	0.310	0.230	0.412	0.628	0.526	0.479	0.584	0.322	0.211	0.211	0.323	0.618	0.531	0.487	0.600	0.018	0.037	0.036	0.018
NDVI (550,780)	0.578	0.400	0.313	0.507	0.674	0.582	0.534	0.632	0.405	0.252	0.251	0.405	0.664	0.587	0.551	0.655	0.026	0.045	0.041	0.023
NDVI (700,800)	0.493	0.327	0.223	0.369	0.618	0.530	0.480	0.578	0.348	0.232	0.231	0.349	0.566	0.497	0.453	0.553	0.036	0.056	0.055	0.036
NDVI (680,900)	0.398	0.222	0.163	0.333	0.508	0.411	0.378	0.476	0.148	0.089	0.091	0.152	0.571	0.474	0.426	0.546	0.001	0.010	0.010	0.002
NDVI (670,800)	0.407	0.229	0.166	0.340	0.509	0.413	0.375	0.471	0.165	0.103	0.105	0.168	0.568	0.472	0.426	0.547	0.002	0.013	0.014	0.014
GNDVI (550,750)	0.575	0.394	0.307	0.504	0.663	0.570	0.520	0.618	0.365	0.219	0.219	0.366	0.665	0.588	0.551	0.654	0.006	0.019	0.017	0.005
NDI1 (680,710,780)	0.525	0.458	0.418	0.495	0.707	0.640	0.621	0.698	0.561	0.408	0.399	0.552	0.380	0.383	0.380	0.382	0.244	0.241	0.237	0.242
NDI2 (680,710,850)	0.518	0.483	0.445	0.488	0.718	0.656	0.641	0.712	0.558	0.406	0.398	0.550	0.406	0.421	0.416	0.406	0.262	0.254	0.251	0.260
NDI3 (715,726,734,747)	0.655	0.593	*	*	0.717	0.696	*	*	0.639	0.516	*	*	0.465	0.439	*	*	0.370	0.384	*	*
DD (670,700,720,750)	0.468	0.379	0.184	0.303	0.654	0.710	0.600	0.664	0.264	0.199	0.196	0.263	0.366	0.372	0.357	0.401	0.021	0.016	0.027	0.034
NW-1 (900,970)	0.835	0.698	*	*	0.741	0.730	*	*	0.598	0.437	*	*	0.467	0.405	*	*	0.021	0.034	*	*
NW-2 (850,970)	0.786	0.626	*	*	0.704	0.705	*	*	0.593	0.435	*	*	0.232	0.198	*	*	0.083	0.101	*	*
NW-3 (920, 970)	0.842	0.715	*	*	0.751	0.737	*	*	0.620	0.454	*	*	0.558	0.492	*	*	0.197	0.233	*	*
NW-4 (880,970)	0.829	0.681	*	*	0.721	0.722	*	*	0.624	0.457	*	*	0.394	0.347	*	*	0.114	0.134	*	*
MSR (670,800)	0.600	0.477	0.397	0.550	0.531	0.486	0.466	0.541	0.128	0.082	0.089	0.140	0.541	0.527	0.525	0.564	0.000	0.006	0.008	0.001
MCARI (550,670,700)	0.204	0.255	0.332	0.263	0.013	0.004	0.003	0.013	0.199	0.117	0.099	0.017	0.032	0.048	0.067	0.047	0.013	0.030	0.019	0.005